PREPARATION OF A HIERARCHICAL PORE ZEOLITE WITH HIGH-TEMPERATURE CALCINATION AND ACID-BASE LEACHING

Chengdong Wang, Jinhong Li*, Xiang Wang, Zhiwei Yang, and Kaiyue Huang

[1]Beijing Key Laboratory of Materials Utilization of Nonmetallic Minerals and Solid Wastes, National Laboratory of Mineral Materials, School of Materials Science and Technology, China University of Geosciences, Beijing 100083, People's Republic of China

Abstract—Microporous structure in zeolite leads to diffusion limitation, which causes coke formation and is harmful to catalytic reactions. Hierarchical zeolite containing primary microporosity and secondary porosity at the meso- and macroscales has received much attention due to its enhanced mass transport. Hierarchical Y zeolites were obtained by treating NH_4-Y zeolite with high-temperature calcining and acid-base leaching. The results demonstrated that the calcined zeolite showed great crystallinity after acid-base leaching. The mechanism of introduction of mesopores was demonstrated in detail. The calcination transformed framework Al to extra-framework Al and enlarged the defect by acid and alkali. The mesopores increased with the calcining temperature and holding time. The relationship between the heating rate and the removal of Al species was non-linear; a heating rate of 100°C/h exhibited good protection for the zeolite structure.

Keywords—Acid site · Acid-base leaching · Calcination · Hierarchical Y zeolite · Pore structure

INTRODUCTION

Zeolite is a critical component in industrial fluidized cracking catalysis (FCC) used widely in petroleum processing (Xu et al. 2007). However, micropores limit the ability of the solid to separate molecules of different sizes (Davis 2002), largely because the increase in side reactions with a large quantity of byproducts (some undesirable mixture of solid particles and catalyst phases) leads to coke formation on the internal surface of micropores, which blocks zeolite pores and channels (Zhang et al. 2006). The limitation of diffusion causes a series of results such as catalyst deactivation and the decrease of catalyst life, the approach to modifying catalytic materials focuses mainly on the following three methods: (1) control of crystallite size (Shiralkar et al. 1991); (2) synthesis of zeolite by taking advantage of the two dimensional (2-D) layered nanostructure (Hermann et al. 2014; Zhou et al. 2016; Wei et al. 2018; Wojtaszek-Gurdak et al. 2019); and (3) establish hierarchical pores by the introduction of mesoporous channels into microporous zeolite (Qin et al. 2011; Moosavifar & Fathyunes 2016). Two or more pore systems (different pore sizes or shapes) in zeolite shorten the diffusion path and minimize the possibility of catalyst deactivation (Hartmann et al. 2016).

Na-Y zeolite has a faujasite-type structure which conforms to a cubic crystal system. The three-dimensional structure is dense and the intrinsic micropores are a twelve-membered ring structure. Some zeolites occur naturally (Zhou & Keeling 2013) but those commonly used for industrial applications are synthesized by hydrothermal processes (Zhao et al. 2016; Galadima & Muraza 2018). The

initial crystallization process, however, is rather inefficient, yielding a product that has low thermal stability, low purity, and low acidity, all of which degrade its catalytic activity by decreasing its stability and diffusional performance (Lee et al. 2017; Fals et al. 2018; Iyoki et al. 2018). Li et al. 2017 found that improved catalytic activity could be achieved by upgrading the mesoporosity of the zeolite to a hierarchical porous system. The synthesis of such a hierarchical system in the zeolite is divided into two main categories. One is `bottom-up' such as hard templating or soft templating, the other is `top-down' which involves dealumination, desiliconization, and recrystallization (Zhao et al. 2016; Feliczak-Guzik 2017). A post-synthesis process removing framework atoms (Al and Si atoms) from the structure is employed to modify the framework structure and change composition (e.g. Si/Al ratio) (Ji et al. 2017). In zeolite, the existence of extra-framework aluminum (EFAL) species is crucial for its catalytic properties (Remy et al. 1996; Triantafillidis et al. 2000; Yu et al. 2010), which is the reason that zeolite is extremely sensitive to variations in Al coordination (Sandoval-Díaz et al. 2015). Dealuminization plays a major role in generating the mesoporous/macroporous framework in zeolite, which not only improves the hydrothermal stability, but also increases the acidity of the zeolite. The EFAL species have an important regulatory effect on the acidity of molecular sieves. In point of fact, free Al ions in zeolite will improve the selectivity of reactant, product, and intermediates. Most Al species in the zeolite can be removed from the framework by heating, substitution, and acid treatment.

The temperature of calcination is an important factor in the generation of a hierarchical structure. Slow cooling gives rise to a zeolite having much better properties such as greater crystallinity and larger pore size (Van Oers et al. 2009). The heating process has a huge impact on the zeolite structure; specificilly the heating rate, calcination temperature, and holding time. The calcination process is the key factor in setting up a mesoporous framework by transforming amino-groups to proton form and by the production of thermal defects. Above all, heat treatment brought about two important side effects (Hong & Fripiat 1995): one is the Si/Al ratio of the zeolite and the other is the porosity. The Al-O tetrahedral structure is less stable than the Si-O tetrahedral structure, so Al can be removed easily from zeolite (Petrovic & Navrotsky 1997). The structural modification results in a change of Al species, which causes a change in the number and strength of acid sites (i.e. Brönsted and Lewis acid). Heat treatment also modifies porosity because of thermal defects, but the nature and number of defects can be controlled by heating rate and holding time. The unstable defect region is easily removed from the zeolite framework by acid-base treatment for the purpose of generating mesopores.

The integrity of the zeolite framework and the number of acid sites for use in catalysis are also important to consider. The purposes of the present study were (1) to synthesize zeolite with a hierarchical structure to obtain multiporosity and multifunctionality by using different procedures to modify Y zeolite, (2) to determine the relationship between the removal of EFAL species and the expansion of mesopores, and (3) to evaluate in detail the structure and acidity of the zeolite products obtained.

EXPERIMENTAL

Materials

Hydrochloric acid (HCl, 37.2 wt.%, Analytical reagent (A.R.)) and sodium hydroxide (NaOH, >96%, A.R.) were purchased from Beijing Chemical Reagent Co., Ltd. China. Ammonium phosphate ($(NH_4)_3PO \cdot 3H_2O$, >98%, A.R.) was purchased from Tianjin Guangfu Fine Chemical Research Institute. The Na-Y faujasite (zeolite) used as the starting raw material was obtained from Yuanli Chemical Engineering Company, Tianjin, China.

Experimental

Zeolite was modified by a post-synthesis process (Fig. 1). The first step in preparing the hierarchical zeolite was to synthesize H-Y zeiolite from the starting raw faujasite. This

was accomplished by ion exchange for three times with $(NH_4)_3PO_4 \cdot 3H_2O$ solutions (0.033 mol/L) at 50°C for 1 h, with a solution-to-zeolite ratio of 20 mL/g. The solid products were collected and dried at 90°C overnight in an oven; zeolite samples were calcined with different heating rates (v_T), calcination temperatures (T_c), and holding times (t_h) (Table 1). Sample DY-0 was used as a reference and was not treated at high temperature. The treated samples were placed in 0.2M HCl at 80°C for 3 h, with a solution-to-zeolite ratio of 30 mL/g. The samples were collected and dried at 90°C overnight in an oven. After dealuminization, base treatment of the modified samples was performed by using 0.2 M NaOH solution at 65°C for 1 h, with a solution-to-zeolite ratio of 30 mL/g. The samples were collected and dried at 90°C overnight in an oven.

Characterization

X-ray diffraction (XRD) was used to determine phase composition of the samples. The samples were analyzed using a Bruker D8 ADVANCE diffractometer (Karlsruhe, Germany) with Cu Kα radiation (λ = 1.5418 Å) operating at 40 kV and 40 mA. The XRD patterns in the scan range 3 to 50°2θ were recorded at room temperature with a scan rate of 10.0°2θ/min.

Chemical compositions were determined by X-ray fluorescence (XRF) using a Rigaku ZSXprimus instrument (Tokyo, Japan). Samples were pressed into discs having 30-mm diameter and they were tested with a Rh target and a 30-mm optical grating.

The morphology was observed by scanning electron microscopy (SEM) using a Hitachi JSM-6700F (Tokyo, Japan) operating at 15 kV (point resolution: 1.5 nm). The powder samples were dispersed on a micro-grid and gold-coated to enhance their electrical conductivity.

To calculate surface area and porosity of samples, Nitrogen (N_2) physisorption measurements were performed at the temperature of liquid N_2 using a Micrometrics ASAP 2460 instrument (Shanghai, China). Prior to measurement, all samples were vacuum-degassed at 350°C for 5 h.

The environments around Al and Si species were characterized by nuclear magnetic resonance (NMR) using a JEOL JNM-ECZ600R instrument (Tokyo, Japan). For the recording of the ^{27}Al and ^{29}Si MAS NMR spectra, a recycle delay of 5 s and a spinning frequency of 14 kHz were used.

In order to observe acid strength of ion-exchanged zeolite and calcined zeolite, NH_3-TPD of the catalysts was performed using a Micrometrics Auto Chem II 2920 (Shanghai, China). The sample was heated to 600°C under a high-purity He flow
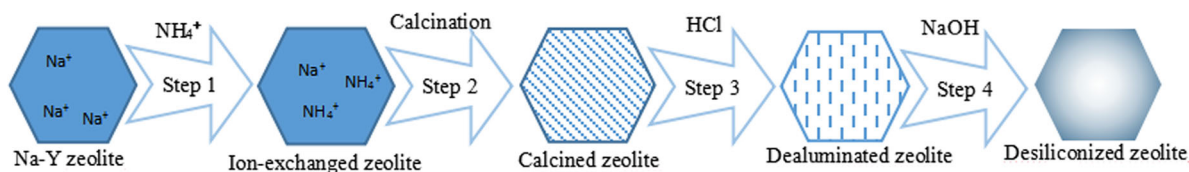

Fig. 1. Schematic of the preparation of hierarchical zeolite by a four-step process

Table 1 Heating treatment parameters and corresponding sample designations of zeolites

Samples	Heating rate (°C/h)	Calcining temperature (°C)	Holding time (h)
DY-1	80	550	3
DY-2	80	550	6
DY-3	100	550	6
DY-4	120	550	6
DY-5	80	600	3
DY-6	80	600	6

and held there for 120 min., then the sample was exposed to NH_3 for 15 min to ensure adsorption saturation. The sample was then cooled to 100°C in a nitrogen atmosphere and held at that temperature for 1 h, then the temperature was raised back to 600°C at a rate of 10°C/min.

Statistical Data Analysis

The crystallinity was calculated (Saepurahman and Hashaikeh 2018; Cui et al. 2019) using Eq. 1:

$$\%Crystallnity = \frac{characteristic\ peak\ areas\ of\ synthesized\ zeolite \times 100\%}{Total\ characteristic\ peaks\ area\ of\ reference\ sample} \quad (1)$$

The Na-Y sample was the reference sample and the diffraction patterns of all samples were measured over the range 3 to

50°2θ. Experimental patterns were analyzed using Jade 6.5 software (MDI, Livermore, California) (Manful et al. 2008) in conjunction with the ICDD (International Centre for Diffraction Data, Newtown Square, Pennsylvania) database to identify the phases revealed by the XRD patterns.

Surface area and porosity were measured using N_2 adsorption and desorption isotherms, and the pore-size distributions between 1.7 and 300 nm were obtained from the Barrett-Joyner-Halenda (BJH) method. The total surface area (S_{total}) of the samples was calculated using Eq. 2:

$$S_{total} = S_{meso} + S_{micro} \quad (2)$$

The amount of Si species present was calculated from the areas of the characteristic peaks for Si in the ^{29}Si MAS NMR spectra of the samples. The framework Si/Al ratio ($F_{Si/Al}$) was estimated from the relative proportion of the total number of Si atoms and Al atoms.

The strength distribution of the acid sites was estimated from deconvolution of the TPD plots using Gaussian curves (Saravanamurugan & Riisager 2013).

RESULTS AND DISCUSSION

The similarity in the XRD patterns of zeolites (Fig. 2) indicates that the original zeolite structure was mostly retained. Strong diffraction peaks appeared at 6.18, 15.61, and 23.64°2θ, corresponding to the (111), (331), and (533) planes, respectively. All samples showed the typical characteristic peaks of FAU zeolite (PDF#12-0228). From XRF (Table 2),
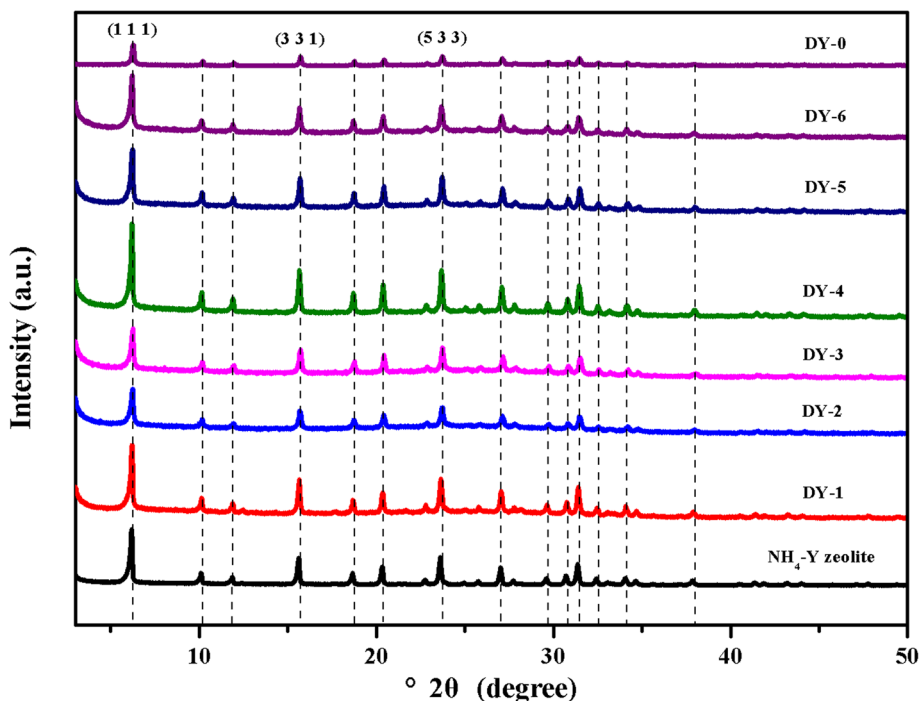
Fig. 2. XRD patterns of the ion-exchange zeolite (NH_4-Y zeolite) and the desiliconized zeolite (DY-0, DY-1, DY-2, DY-3, DY-4, DY-5, and DY-6)

Table 2 Composition (wt.%) of NH_4-Y zeolite and calcined zeolite

Component	Na_2O	Al_2O_3	SiO_2	P_2O_5	Impurity
NH_4-Y zeolite	4.22	23.6	71.7	0.0141	0.466
Calcined zeolite	4.33	23.8	71.5	0.0153	0.355

no extra elements (in addition to the elements in the NH_4-Y zeolite) were found in the calcined zeolite structure. The measurements indicated that the zeolite had no obvious composition change during the calcination process.

Crystallinity measurements (Table 3) revealed changes in the crystallinity of the modified zeolite. The relative crystallinity of dealuminated zeolite without thermal treatment (DY-0) was only 32% of the NaY sample, which confirmed that the structure was damaged seriously. The high concentration HCl solution resulted in the collapse of the zeolite framework and reduced the crystallinity, but the dealuminated zeolites with calcination (DY-1, DY-2, DY-5, and DY-6) maintained most (93–98%) of the crystal structure of the NaY sample. The crystal structure stability of calcined zeolite was better than the zeolite without calcination in acid solution. After calcination, the crystallinity values of calcined zeolite were decreased distinctly but the relative crystallinity of dealuminated zeolite with acid treatment was increased slightly. With the whole treatment, the crystallinity of desiliconized zeolite (except for DY-0) showed an obvious reduction when compared with dealuminated zeolite. The contrast among the desiliconized zeolites (DY-1, DY-2, DY-5, and DY-6) showed more amorphous phases because of the higher heating temperature and longer holding time.

As reveal by the ^{27}Al MAS NMR signal (Fig. 3), the Al element in the NH_4-Y zeolite consisted only of FAL species. The peak at 60 ppm was attributed to four-coordinate Al (Al-O tetrahedron). The result was consistent with the crystallinity calculated from XRD analysis. Though the zeolite was treated with $(NH_4)_3PO_4$ solution, the zeolite structure was maintained

Table 3 Crystallinity of modified zeolite by heat treatment with different heating temperatures and holding times[a]

Samples[b]	X_c	X_a	X_b
DY-0		32.0	80.1
DY-1	87.0	96.2	93.2
DY-2	90.6	95.1	86.3
DY-5	91.6	93.7	96.4
DY-6	93.3	98.0	94.5

X_c: The crystallinity of calcined zeolite

X_a: The crystallinity of zeolite treated by acid

X_b: The crystallinity of zeolite treated by base

[a] The relative crystallinity of NH_4-Y was 99.8%

[b] All the samples were treated with heating rate of 80°C /h (except for DY-0)

well. After heat treatment, a new peak at –1.849 ppm, which was attributed to six-coordinate Al (Al-O octahedron), appeared in the zeolite. The Al-O tetrahedron as FAL species existed in the ion-exchanged zeolite structure. After heat treatment, a new kind of EFAL species (six-coordinate Al) was generated. Contrasting the total characteristic peak areas of ion-exchanged zeolite with calcined zeolite revealed that free Al ions were generated in the calcined zeolite. EFAL species existed in the framework in both the complex and the free states such as Al^{3+}, AlO^+, $AlO(OH)$, and $Al(OH)_3$ (Scherzer 1984).. In the ^{29}Si MAS NMR spectrum (Fig. 4), the peaks were assigned to (Si(4Al)), (Si(3Al)), (Si(2Al)), (Si(1Al)), and (Si(0Al)) environments. Si atoms connect to four T (Si or Al) atoms by bridging oxygens; and nAl (n = 0, 1, 2, 3, 4) indicated the number of aluminum atoms in the second coordination shell. The Si species in ion-exchanged zeolite consisted of all types of Si species. Compared with the ^{29}Si MAS NMR spectrum of ion-exchanged zeolite, the peaks in the calcined zeolite were displaced by 2 ppm. After calcining, the Si species (Si(4Al)) and (Si(3Al)) almost all disappeared. The bonds connecting Si with four Al atoms all broke, which may mean that some of the transformed Si species were extra-framework (EFSI).

Some EFSI and EFAL species existed as amorphous phases in the zeolite, which was the reason the crystallnity of ion-exchanged zeolite decreased after calcination (Table 3). The zeolite crystallinity increased after acid treatment, which indicated that the amorphous phases were dissolved by the acid. Calcination influenced the zeolite structure by the formation of defects, which were then more susceptible to acid or base attack resulting in enlargement of the pore size in the sample. Acid treatment removed some of the EFAL or EFSI species, and the crystal structure was optimized to a degree.

The ^{29}Si MAS NMR spectra of desiliconized zeolite and dealuminated zeolite were interpreted by assigning the peaks to (Si(3Al)), (Si(2Al)), (Si(1Al)), and (Si(0Al)) species (Fig. 5). The Si species in zeolite which had been modified by calcination and acid leaching consisted of three types: (Si(2Al)), (Si(1Al)), and (Si(0Al)). After base leaching, the amount of Si species in zeolite decreased and a new Si species (Si(3Al)) was generated. The framework ratio of Si/Al calculated from the ^{29}Si NMR spectrum and the percentage of each Si species were revealed in the ^{29}Si MAS NMR data (Table 4). The decrease in (Si(1Al)) and (Si(0Al)) species and the increase in (Si(3Al)) and (Si(2Al)) species indicated that part of the zeolite framework was destroyed. Some of Si-O-Si bonds were broken, thus enabling Si atoms to connect to Al atoms through bridging oxygens during alkaline treatment.

SEM images (Fig. 6a) showed that the integrity of the structure of the ion-exchanged zeolite was good. The SEM images (Fig. 6) and hysteresis loop (Fig. 7) indicated that the surface in dealuminated zeolite had no or only a few pores. After alkaline leaching, the mesopores appeared in the zeolite.

The hysteresis loop in the N_2 adsorption isotherms of the acid-treated zeolite exhibited type I behavior (Fig. 7a), which indicated that dealuminated zeolites had few mesopores and the pores were composed almost entirely of micropores (Fig.
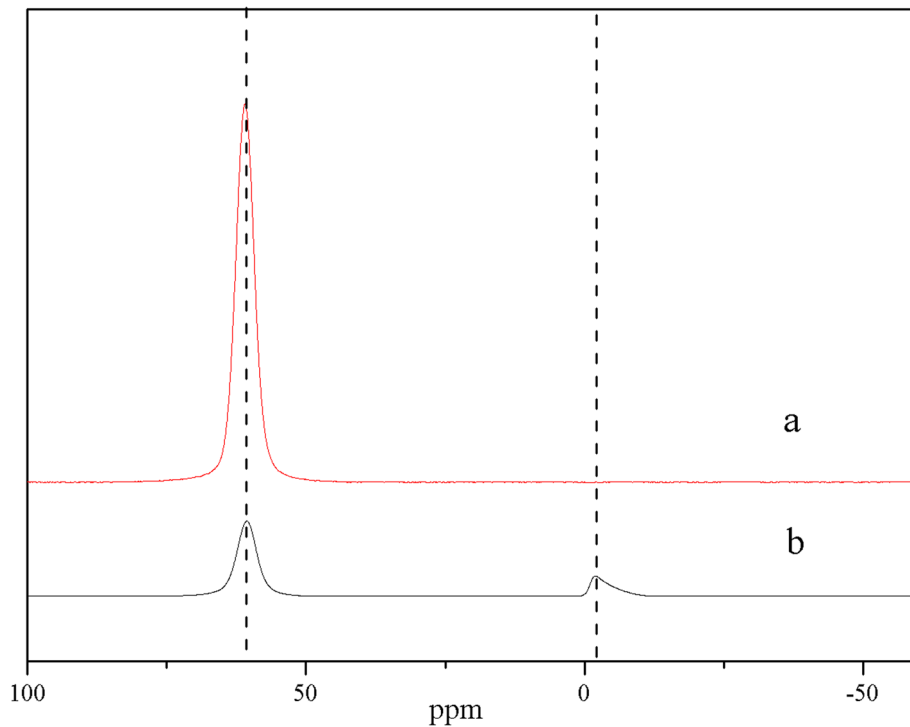
Fig. 3. The ^{27}Al MAS NMR spectrum of (a) ion-exchanged zeolite and (b) calcined zeolite

8a). The hysteresis loop of desiliconized zeolites (Fig. 7b), on the other hand, showed that mesopores were enlarged by alkaline treatment.

Pore-size distributions (Fig. 8) revealed that the framework in the modified zeolites was composed mainly of a hierarchical structure with many mesopores (Fig. 8b). A peak at 3–5 nm
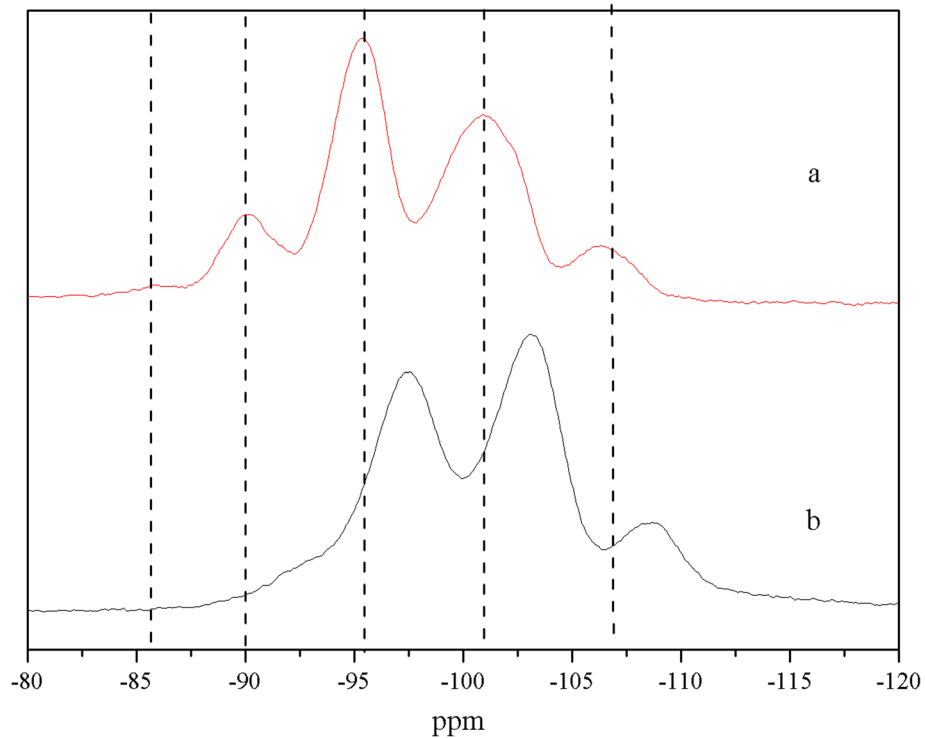
Fig. 4. The ^{29}Si MAS NMR spectrum of (a) ion-exchanged zeolite and (b) calcined zeolite
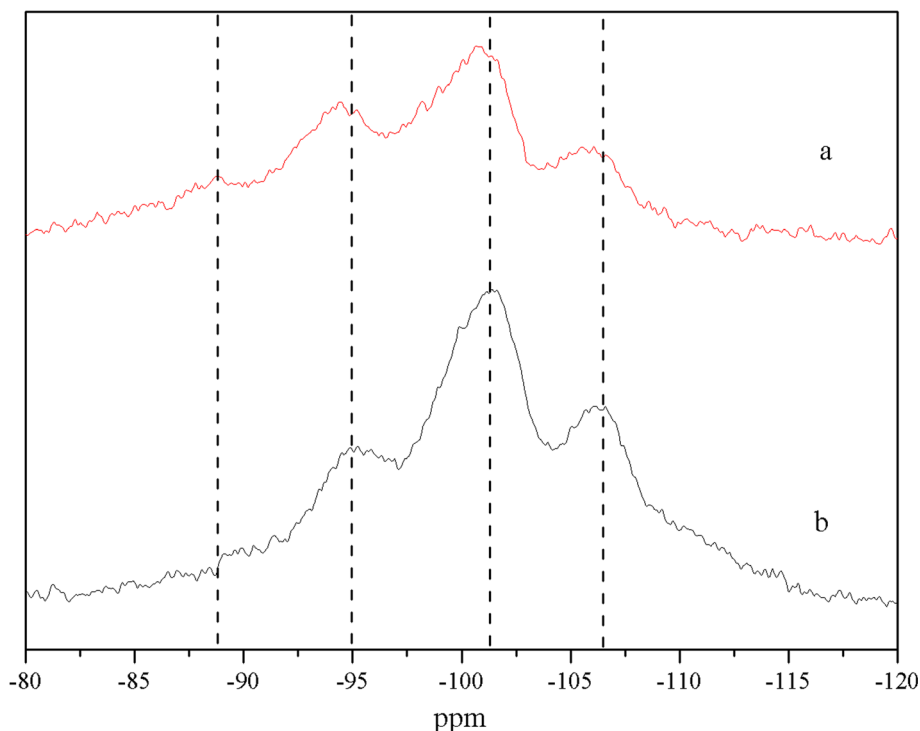
Fig. 5. The ^{29}Si MAS NMR spectrum of (a) desiliconized zeolite and (b) dealuminated zeolite

appeared in DY-5 with a calcining temperature of 600°C using an aperture distribution chart. However, the peak at 3–5 nm disappeared (DY-6) when the holding time increased from 3 h to 6 h, which meant the framework in DY-6 collapsed so seriously during a long period of calcination that HCl could not clear the pore channels. The collapse of the zeolite framework caused by high temperature and long heating time resulted in the blocking of mesopores and an overall decrease in effective pore size. The blocked structure, however was cleaned when subjected to alkaline leaching.

From the surface area and pore volume data (Table 5), the specific surface area of the zeolite samples apparently became smaller because of increasing mesoporosity and decreasing microporosity after acid-base leaching. Comparing all samples, high temperature and long holding time caused serious damage to the zeolite structure (DY-1, DY-2, DY-5, and DY-6). After acid-base leaching, the framework of the zeolites exposed to a heating rate of 80°C/h, a calcining temperature of 600°C, and a holding time of 6 h were very seriously damaged, and the volume of micropores was only 0.002 cm^3/g. A large number of micropores were enlarged to mesopores, even to macropores, which was harmful for a suitable environment for chemical reaction. The desiliconized zeolite treated at different

heating rates (DY-2, DY-3, and DY-4) showed a particular phenomenon: when the heating rate was 80°C/h (DY-2) or 120°C/h (DY-4) the surface area of desiliconized zeolite was ~180 m^2/g, but that of sample DY-3 (100°C/h) was 317.9 m^2/g, which was far larger than the former. DY-3 showed the best protection for a zeolite framework when comparing the micropore and mesopore volumes of the three samples.

The differences in acidity between ion-exchanged zeolites and calcined zeolites are shown in the NH$_3$-TPD images (Fig. 9). The peaks were classified and attributed to three types of acid sites with different acidic strengths (The three peaks from left to right represent weak, medium and strong, respectively) by Gaussian curves, and the number of acid sites (mmol of NH$_3$/g of hydrated sample) was calculated (Table 6). Calcining at high temperature for a long time transformed the zeolite from NH$_4$-Y to H-Y, and the total number of acidic sites was clearly decreased. Combining with the composition of NH$_4$-Y zeolite and calcined zeolite (Table 2), phosphate ions (PO3- 4) in calcined samples had little influence on acid sites. Treated with different variables (heating rate, calcining temperature, and holding time), the amount of acid sites data with different strength changed. High temperature (DY-5 and DY-6) and long holding time (DY-2 and DY-6) caused a reduction in the

Table 4 ^{29}Si MAS NMR data of the samples

	Framework$_{Si/Al}$	Si(3Al)%	Si(2Al)%	Si(1Al)%	Si(0Al)%
Dealuminated zeolite	4.04	0.00%	22.02%	54.89%	23.09%
Desiliconized zeolite	3.11	9.14%	29.24%	42.90%	18.71%
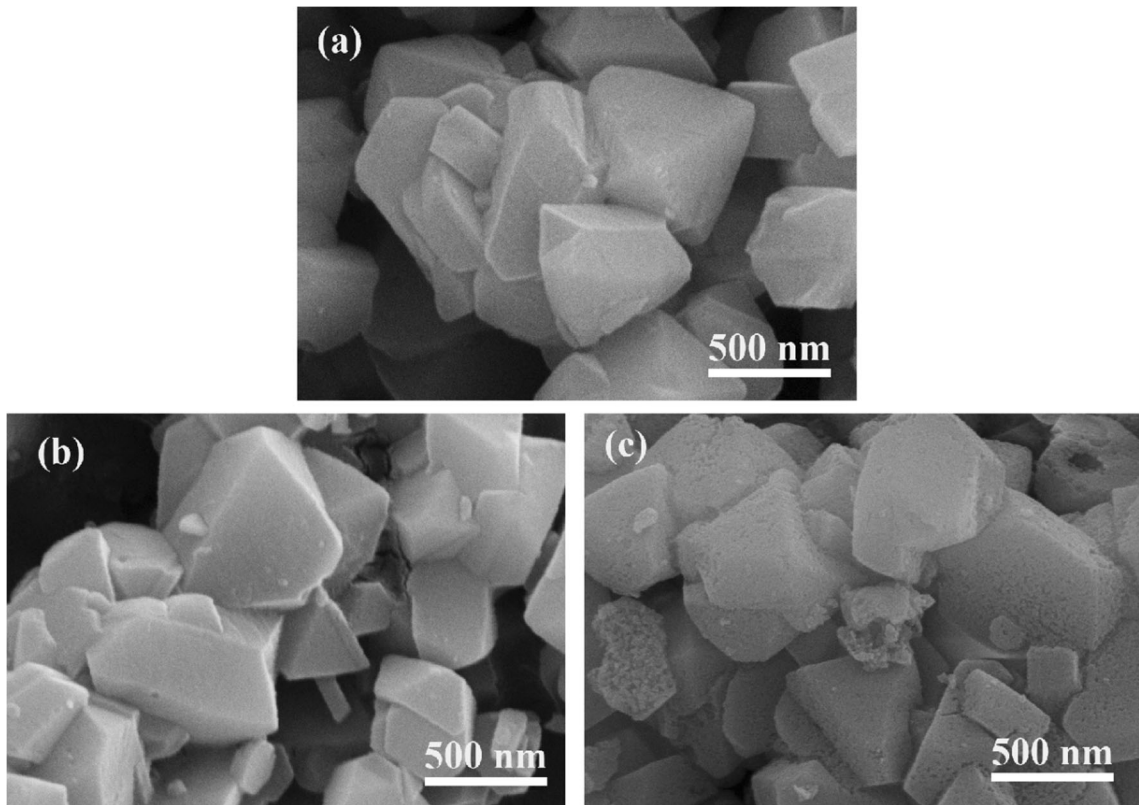
Fig. 6. SEM images of DY-6: (**a**) ion-exchanged zeolite, (**b**) dealuminated zeolite, and (**c**) desiliconized zeolite

number of weak acid sites. The trend was the same with the specific surface area of micropores in zeolite, which meant that the provision of weak acid sites was related to the zeolite framework. Actually, the ratio (strong acid sites/total acid sites) increased during heat treatment. However, an overall loss of acid sites caused by excessive temperature for a long time was harmful for zeolite as a cracking catalyst. Comparing DY-2,

DY-3, DY-4, and NH_4-Y, the number of strong acid sites increased slightly because calcination broke Si-O-Al bonds and transformed Al-O tetrahedra to EFAl species such as Al-O octahedra (**Fig.** 3). In the sample DY-3, more weak acid sites were preserved, which confirmed that a suitable heating rate was beneficial in protecting acidity in the zeolite. The loss of weak and medium acid sites with the degree of dealumination
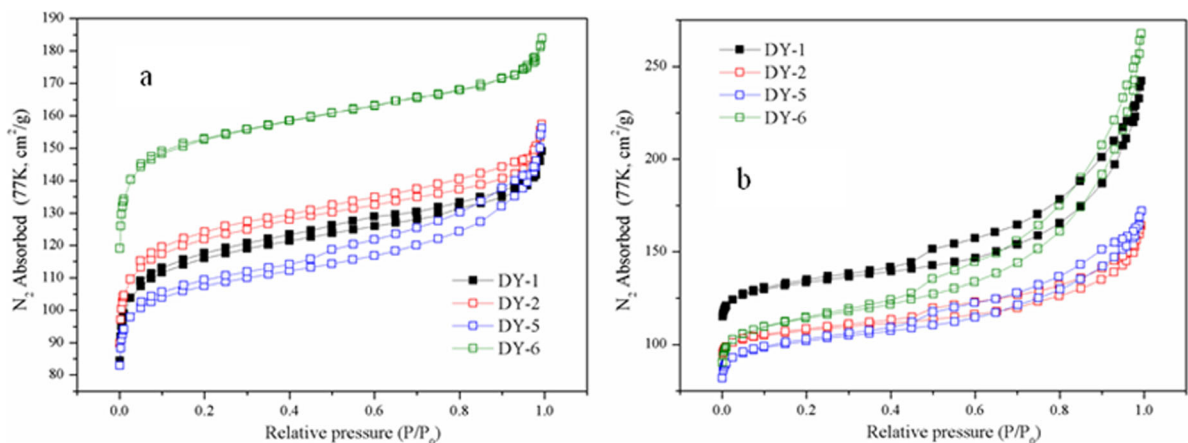
Fig. 7. Hysteresis curve in N_2 isotherm of (**a**) dealuminated zeolites and (**b**) desiliconized zeolites
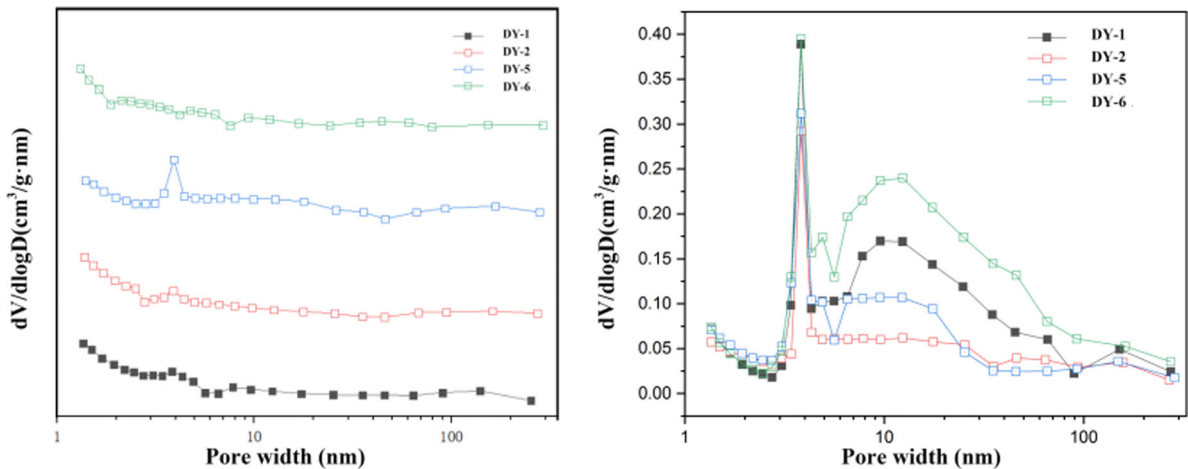
Fig. 8. Pore size distribution of (**a**) dealuminated zeolites and (**b**) desiliconized zeolites by BJH desorption

was related to the corrosion of the microporous structure. Though more mesopores were generated in the DY-6, the significant reduction of acid sites would damage zeolite catalytic activity. A relatively complete structure could prevent the loss of acid sites.

CONCLUSIONS

In this study, modified zeolite samples were prepared by high-temperature calcining and acid-base leaching in order to obtain a hierarchical zeolite with a three-dimensional pore structure. Based on the above discussion, the conclusions were as follows:

(1) The result showed that zeolite (DY-0) crystallinity dropped to 80% and the other (DY-1, DY-2, DY-5 and DY-6) dropped to 85–95% after the whole treatment. Comparing the modified zeolite samples, treatment at the higher temperature caused cleaner zeolite structure.

(2) According to the results of NMR and SEM, high-temperature calcination played an important role in the synthesis of a hierarchical zeolite, the structure of which consists of micropores and mesopores. During calcination, four-coordinate Al in NH$_4$-Y zeolite was transformed to six-coordinate Al as EFAL species, and some Si atoms were connected to Al by oxygen bridges. This phenomenon caused loss of zeolite crystallinity and the appearance of numerous thermal defects, which was an effective way to generate more mesopores. A fast heating rate and short holding time restricted the generation of thermal defects.

(3) High-temperature calcining and acid-base leaching caused a reduction in the specific surface area of zeolite samples. With an increase in calcining temperature and holding time, the damage to the zeolite structure became more serious and the proportion of mesoporous structure in zeolite increased. However, treatment at a suitable heating rate was beneficial to the zeolite structure.

(4) The acid sites were related to calcination. During this process, the $R_{s/t}$ ($R_{s/t}$ = the amount of strong acid sites/ the amount of total acid sites) increased from 0.31 to

Table 5 Surface areas and pore volumes NH$_4$-Y and all the desiliconized Y zeolites involved

| Samples	S_{total}[a] (m^2/g)	S_{micro}[b] (m^2/g)	S_{micro}/S_{total}	V_{micro}[c] (cm^3/g)	V_{meso}[d] (cm^3/g)	V_{micro}/V_{meso}
NH$_4$-Y	515.5	471.5	0.915	0.231	0.031	7.452
DY-0	67.46	36.35	0.539	0.018	0.062	0.290
DY-1	269.8	238.3	0.883	0.117	0.033	3.545
DY-2	181.7	131.7	0.725	0.064	0.126	0.508
DY-3	317.9	275.7	0.867	0.135	0.128	1.055
DY-4	180.9	162.7	0.899	0.080	0.023	3.478
DY-5	231.1	197.3	0.854	0.097	0.101	0.960
DY-6	64.85	5.799	0.089	0.002	0.226	0.009

[a] Total surface area obtained from BET

[b] T-plot Micropore surface area

[c] T-plot Micropore volume

[d] Mesopore volume obtained by BJH method
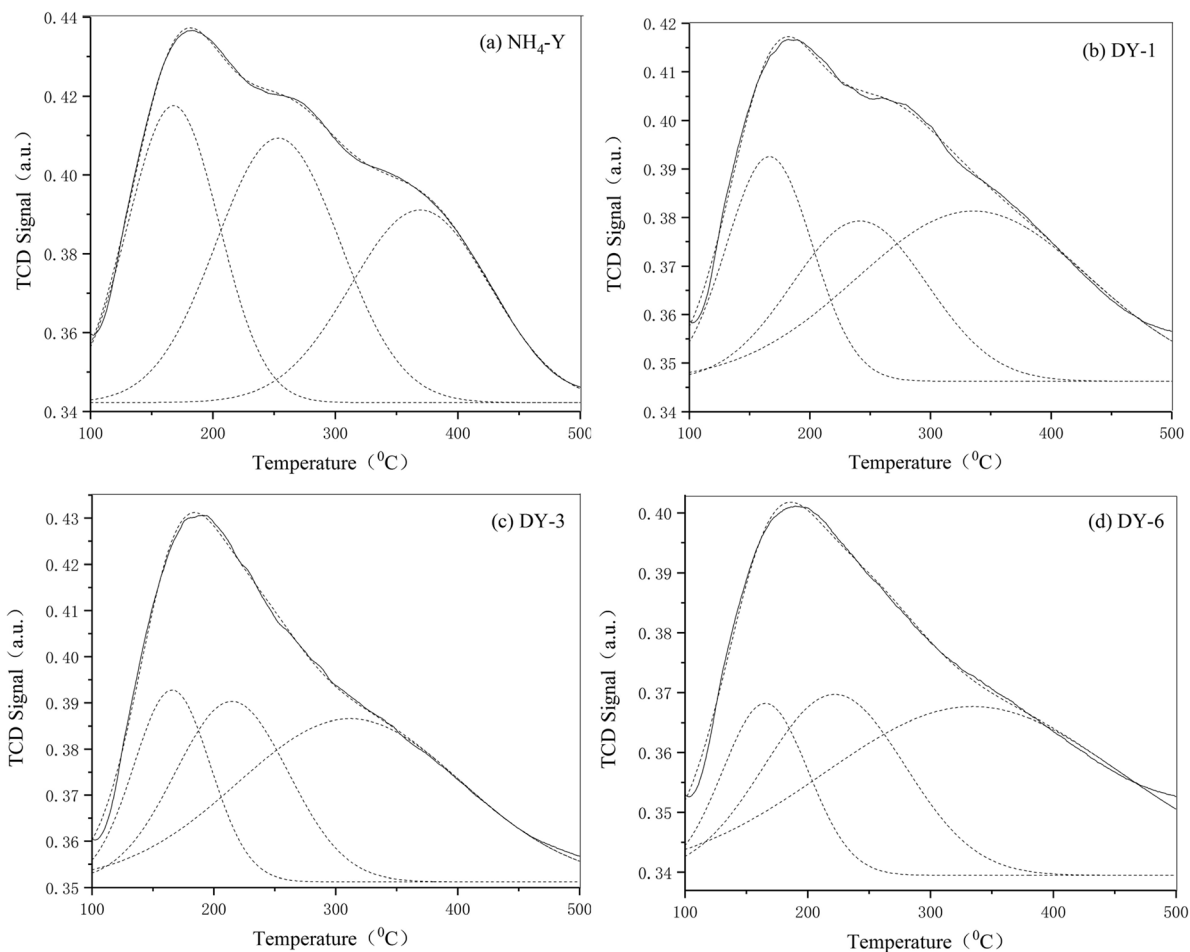
Fig. 9. Experimental (——) and deconvoluted (——) NH₃-TPD curves of Y zeolite samples (**a**) NH₄-Y, (**b**) DY-1, (**c**) DY-3, and (**d**) DY-6

0.50. However, the number of weak and medium acid sites decreased during calcination. Comparison of DY-2, DY-3, and DY-4 revealed that acid sites could be protected with a relatively complete structure when treated with a suitable calcination process.

Table 6 Acid sites of NH₄-Y zeolite and calcined zeolites

Samples	The amount of acid sites (mmol/g)[a] (±0.05)				$R_{s/t}$[c]
	Total	Weak	Medium	Strong	
NH₄-Y	3.07	0.94 (168)[b]	1.18 (253)	0.95 (369)	0.31
DY-1	1.96	0.47 (166)	0.54 (241)	0.95 (336)	0.48
DY-2	1.88	0.26 (159)	0.58 (207)	1.04 (307)	0.54
DY-3	2.04	0.42 (166)	0.59 (215)	1.03 (312)	0.51
DY-4	1.94	0.24 (158)	0.69 (208)	1.01 (313)	0.52
DY-5	1.82	0.36 (171)	0.50 (236)	0.96 (340)	0.53
DY-6	1.35	0.23 (166)	0.40 (222)	0.72 (335)	0.53

[a] Sample = crystalline zeolite + amorphous material produced during calcination

[b] The numbers in parentheses represent the temperature peak maxima at degrees Celsius of the individual desorption steps

[c] $R_{s/t}$= the amount of strong acid sites/the amount of total acid sites

REFERENCES

Cui, Q., Wang, S., Wei, Q., Mu, L., Yu, G., Zhang, T., & Zhou, Y. (2019). Synthesis and characterization of Zr incorporated small crystal size Y zeolite supported NiW catalysts for hydrocracking of vacuum gas oil. *Fuel, 237*, 597–605.

Davis, M. E. (2002). Ordered porous materials for emerging applications. *Nature, 417*, 813–821.

Fals, J., García, J. R., Falco, M., & Sedran, U. (2018). Coke from SARA fractions in VGO. Impact on Y zeolite acidity and physical properties. *Fuel, 225*, 26–34.

Feliczak-Guzik, A. (2017). Hierarchical zeolites: synthesis and catalytic properties. *Microporous & Mesoporous Materials, 259*, S138718111730642X.

Galadima, A., & Muraza, O. (2018). Hydrocracking catalysts based on hierarchical zeolites: a recent progress. *Journal of Industrial and Engineering Chemistry, 61*, 265–280.

Hartmann, M., Machoke, A. G., & Schwieger, W. (2016). Catalytic test reactions for the evaluation of hierarchical zeolites. *Chemical Society Reviews, 45*, 3313.

Hermann, J., Trachta, M., Nachtigall, P., & Bludský, O. (2014). Theoretical investigation of layered zeolite frameworks: surface properties of 2D zeolites. *Catalysis Today, 227*, 2–8.

Hong, Y., & Fripiat, J. J. (1995). Microporous characteristics of H-Y, H-ZSM-5 and H-mordenite dealuminated by calcination. *Microporous Materials, 4*, 323–334.

Iyoki, K., Yamaguchi, Y., Endo, A., Yonezawa, Y., Umeda, T., Yamada, H., Yanaba, Y., Yoshikawa, T., Ohara, K., & Yoshida, K. (2018) Formation of a dense non-crystalline layer on the surface of zeolite Y crystals under high-temperature steaming conditions. *Microporous & Mesoporous Materials, 268*.

Ji, D., Liu, H., Wang, X., Liu, H., Gao, X., Xu, C., & Wei, S. (2017) Mesostructured Y zeolite from NaY with low Si/Al by one-step method based on bifunctional surfactant. *Materials Chemistry & Physics, 196*.

Lee, K., Lee, S., Jun, Y., & Choi, M. (2017). Cooperative effects of zeolite mesoporosity and defect sites on the amount and location of coke formation and its consequence in deactivation. *Journal of Catalysis, 347*, 222–230.

Li, C., Guo, L., Liu, P., Gong, K., Jin, W., Li, L., Zhu, X., Liu, X., Shen, B. (2017) Defects in AHFS-dealuminated Y zeolite: a crucial factor for mesopores formation in the following base treatment procedure. *Microporous & Mesoporous Materials, 255*.

Manful, J. T., Grimm, C. C., Gayin, J., & Coker, R. D. (2008). Effect of variable parboiling on crystallinity of rice samples. *Cereal Chemistry, 85*, 92–95.

Moosavifar, M., & Fathyunes, L. (2016). Influence of the post-synthesis method on the number and size of secondary mesoporous structure of NaY zeolite and its effect on catalyst loading. An efficient and eco-friendly catalyst for synthesis of xanthenes under conventional heating. *Journal of the Iranian Chemical Society, 13*, 1–8.

Petrovic, I., & Navrotsky, A. (1997). Thermochemistry of Na-faujasites with varying Si/Al ratios. *Microporous Materials, 9*, 1–12.

Qin, Z., Shen, B., Gao, X., Lin, F., Wang, B., & Xu, C. (2011). Mesoporous Y zeolite with homogeneous aluminum distribution obtained by sequential desilication–dealumination and its performance in the catalytic cracking of cumene and 1,3,5-triisopropylbenzene. *Journal of Catalysis, 278*, 266–275.

Remy, M. J., Stanica, D., Poncelet, G., Feijen, E. J. P., Grobet, P. J., Martens, J. A., & Jacobs, P. A. (1996). Dealuminated H-Y zeolites: relation between physicochemical properties and catalytic activity in heptane and decane isomerization. *The Journal of Physical Chemistry, 100*, 12440–12447.

Saepurahman, & Hashaikeh, R. (2018). Insight into ball milling for size reduction and nanoparticles production of H-Y zeolite. *Materials Chemistry and Physics, 220*, 322–330.

Sandoval-Díaz, L.-E., González-Amaya, J.-A., & Trujillo, C.-A. (2015). General aspects of zeolite acidity characterization. *Microporous & Mesoporous Materials, 215*, 229–243.

Saravanamurugan, S., & Riisager, A. (2013). Zeolite catalyzed transformation of carbohydrates to alkyl levulinates. *ChemCatChem, 5*, 1754–1757.

Scherzer, J. (1984) *Catalytic materials: Relationship between structure and reactivity.* ACS Symposium Series, 157–200 pp.

Shiralkar, V. P., Joshi, P. N., Eapen, M. J., & Rao, B. S. (1991). Synthesis of Zsm-5 with variable crystallite size and its influence on physicochemical properties. *Zeolites, 11*, 511–516.

Triantafillidis, C. S., And, A. G. V., & Evmiridis, N. P. (2000). Dealuminated H−Y zeolites: influence of the degree and the type of dealumination method on the structural and acidic characteristics of H−Y zeolites. *Industrial & Engineering Chemistry Research, 39*, 307–319.

Van Oers, C. J., Stevens, W. J. J., Bruijn, E., Mertens, M., Lebedev, O. I., Van Tendeloo, G., Meynen, V., & Cool, P. (2009). Formation of a combined micro- and mesoporous material using zeolite beta nanoparticles. *Microporous & Mesoporous Materials, 120*, 29–34.

Wei, R., Yang, H., Scott, J. A., Aguey-Zinsou, K., & Zhang, D. (2018). Synthesis of 2D MFI zeolites in the form of self-interlocked nanosheet stacks with tuneable structural and chemical properties for catalysis. *Applied Materials Today, 11*, 22–33.

Wojtaszek-Gurdak, A., Zielinska, M., & Ziolek, M. (2019). MWW layered zeolites modified with niobium species-surface and catalytic properties. *Catalysis Today, 325*, 89–97.

Xu, B., Bordiga, S., Prins, R., & Bokhoven, J. A. V. (2007). Effect of framework Si/Al ratio and extra-framework aluminum on the catalytic activity of Y zeolite. *Applied Catalysis A General, 333*, 245–253.

Yu, Z. W., Zheng, A. M., Wang, Q. A., Chen, L., Xu, J., Amoureux, J. P., & Deng, F. (2010). Insights into the dealumination of zeolite HY revealed by sensitivity-enhanced Al-27 DQ-MAS NMR spectroscopy at high field. *Angewandte Chemie-International Edition, 49*, 8657–8661.

Zhang, X. J., Wang, Y., & Xin, F. (2006). Coke deposition and characterization on titanium silicalite-1 catalyst in cyclohexanone ammoximation. *Applied Catalysis A: General, 307*, 222–230.

Zhao, J., Wang, G., Qin, L., Li, H., Chen, Y., & Liu, B. (2016). Synthesis and catalytic cracking performance of mesoporous zeolite Y. *Catalysis Communications, 73*, 98–102.

Zhou, C., & Keeling, J. (2013). Fundamental and applied research on clay minerals: From climate and environment to nanotechnology. *Applied Clay Science, 74*, 3–9.

Zhou, C., Zhao, L., Wang, A., Chen, T., & He, H. (2016). Current fundamental and applied research into clay minerals in China. *Applied Clay Science, 119*, 3–7.